Astron. Astrophys. 207, 1–15 (1988)

ASTRONOMY AND ASTROPHYSICS

The radial distribution of galactic gamma rays

IV. The whole Galaxy

A.W. Strong[1], J.B.G.M. Bloemen[2,4,6], T.M. Dame[7], I.A. Grenier[3], W. Hermsen[4], F. Lebrun[3], L.-Å. Nyman[7], A.M.T. Pollock[5], and P. Thaddeus[7]

[1] Max-Planck Institut für Physik und Astrophysik, Institut für Extraterrestrische Physik, D-8046 Garching, Federal Republic of Germany
[2] Department of Astronomy, University of California, Berkeley, CA 94720, USA
[3] Service d'Astrophysique, Centre d.'Etudes Nucleaires de Saclay, France
[4] Laboratory for Space Research, Leiden, The Netherlands
[5] EXOSAT Observatory, Space Science Department of the European Space Agency, ESTEC, Noordwijk, The Netherlands
[6] Leiden Observatory, Leiden, The Netherlands
[7] Harvard-Smithsonian Centre for Astrophysics, Cambridge, MA 02138, USA

Received February 23, accepted May 10, 1988

Summary. The correlation between diffuse galactic γ-rays and gas tracers is studied using the final COS-B database and H I and CO surveys covering the entire galactic plane. A good quantitative fit to the γ-rays is obtained, with a small gradient in the γ-ray emissivity per hydrogen atom. The average ratio of H_2 column density to integrated CO temperature is determined, the best estimate being $2.3 \pm 0.3\ 10^{20}$ molecules cm^{-2} (K km $s^{-1})^{-1}$. (This value is an upper limit if a population of unresolved γ-ray sources exists with an angular distribution similar to that of the molecular gas, or if the cosmic-ray density is enhanced in molecular clouds). The corresponding mass of molecular hydrogen in the inner Galaxy, derived using both 1st and 4th quadrants, is $1.0\ 10^9\ M_\odot$.

It is shown on a statistical basis that the softer γ-ray spectrum towards the inner Galaxy found in previous work can be attributed to a steeper emissivity gradient at low energies and/or to a softer γ-ray spectrum of the emission distributed like molecular gas. Our statistical tests suggest the latter is probably the better model. A steeper emissivity gradient at low energies could be related to cosmic-ray spectral variations in the Galaxy, to different distributions of cosmic-ray electrons and nuclei, or to a contribution from discrete sources. A softer spectrum for the emission associated with molecular clouds may be physically related to the clouds themselves (i.e. cosmic-ray spectral variations) or to an associated discrete source distribution.

Key words: COS-B – gamma rays – cosmic rays – interstellar clouds

1. Introduction

The good quantitative correlation between galactic γ-rays and gas tracers (H I and CO emission) in the Galaxy is the main evidence that interactions of cosmic rays with interstellar gas are responsible for most of the diffuse galactic γ-ray emission for energies between 100 MeV and a few GeV. Prior to 1982 it was impossible fully to exploit this correlation for lack of adequate coverage (in particular in *latitude*) in the CO surveys, necessary because of the relatively low angular resolution of γ-ray telescopes. The situation improved dramatically with the availability of the first large-scale 'superbeam' surveys in CO from the Columbia 1.2 m telescope, since they provide complete sampling over a large enough latitude range to allow a reliable comparison with the γ-ray data.

Lebrun et al. (1983) used Columbia CO data (Dame, 1983, Dame and Thaddeus, 1985) and H I data to analyse the γ-ray emission observed by COS-B above 300 MeV in the first galactic quadrant and to place limits on the CO-to-H_2 conversion factor. In this analysis the density of cosmic rays (in this energy range mainly nucleons are involved) was assumed to be uniform in the Galaxy.

In papers I and II of the present series (Bloemen et al., 1984a, b) the correlation between the H I and γ-ray distributions beyond the solar circle (2nd and 3rd quadrants) was studied, ignoring molecular gas. The analysis of Paper III (Bloemen et al., 1986; see also Bloemen, 1985) used low-latitude COS-B data taken from the first 55 (out of 65) observation periods together with the 1st and 2nd quadrant and Carina Columbia CO surveys, and various H I surveys. The latitude range used, $-4.5° < b < 6.5°$, has essentially complete CO coverage in these quadrants. The gas surveys were first divided into galacto-centric distance bins using the rotation curves of Gordon and Burton (1976) and Blitz et al. (1980), as modified by Kulkarni et al. (1982); the bins chosen were 2–8, 8–10, 10–15 and >15 kpc. The analysis was done in three energy ranges and allowed for spatial variations in γ-ray emissivity.

In Paper III the main result was the determination of the γ-ray emissivity gradients in the three energy ranges, the establishment of the requirement for an energy-dependent model, and the derivation of a value for the CO-to-H_2 conversion factor together with a new estimate for the mass of molecular hydrogen in the

Send offprint requests to: A.W. Strong

inner Galaxy. The emissivity gradients were found to be surprisingly small, especially at high energies (>300 MeV), when compared to the distribution of candidate cosmic-ray sources in the Galaxy.

Several developments have now made it possible to improve the analysis of Paper III. These include the availability of the total COS-B database with its final calibration and the updating of the CO database to include the 3rd and 4th quadrants, a new 1st quadrant survey and various other new surveys from the Columbia telescopes. The new CO surveys, as well as covering the entire longitude range, now allow the analysis of a greater latitude range than before. In addition the fitting and error analysis has been refined to allow the rapid appraisal of models even when the number of parameters is large.

An important and independent indication that the underlying assumption is correct, viz, that the bulk of the γ-ray emission originates in interactions of cosmic rays with gas, is provided by the observation of γ-rays from the Orion cloud complex (Bloemen et al., 1984c). The derived ratio of molecular hydrogen column density to integrated CO brightness temperature was $2.6 \pm 1.2\,10^{20}$ molecules cm^{-2} (K km s^{-1})$^{-1}$, which is in agreement with the large-scale analysis (see Sect. 4) and indicates that γ-ray sources are not playing a major role. Similarly studies at intermediate latitudes (Strong et al., 1982a; Strong, 1985a; Strong et al., 1985) show that most of the emission can be explained as the sum of emission from atomic and molecular gas (plus a small inverse Compton component).

2. Method

The method is the same as in Paper III; it consists of fitting the γ-ray data to the function:

$$I_\gamma = \sum_i \frac{q_i}{4\pi} (\tilde{N}_{\mathrm{H\,I},i} + 2Y\tilde{W}_{\mathrm{CO},i}) + f_{\mathrm{IC}}\tilde{I}_{\mathrm{IC}} + I_{\mathrm{B}}^0 + \sum_k f_k I_k, \qquad (1)$$

where q_i is the γ-ray emissivity in the i'th ring, $N_{\mathrm{H\,I},i}$ is the column density of atomic hydrogen, $W_{\mathrm{CO},i}$ is the velocity-integrated CO brightness temperature, Y is the apparent γ-ray value for the conversion factor from CO integrated temperature to H_2 column density, (assuming that q_i applies equally to atomic and molecular gas), $f_{\mathrm{IC}} I_{\mathrm{IC}}$ is the inverse-Compton emission, I_{B}^0 is an isotropic background (cosmic + instrumental) corrected for temporal and angular variations (see Strong et al., 1987 for details), f_k is the flux of the k'th point source included in the model, I_k is the distribution for a source of unit strength situated at the k'th source. The tilde indicates the convolution with the COS-B point-spread function, which is quite accurately known from pre-launch calibrations and studies of the Vela pulsar (see Mayer-Hasselwander, 1985). The free parameters of the model are, for each energy range: $q_{i,i=1-6}$, Y, f_{IC}, I_{B}^0 and $f_{k,k=1-4}$.

The galactocentric rings chosen for the present analysis were: 2–4, 4–8, 8–10, 10–12, 12–15 and >15 kpc (we take $R_\odot = 10$ kpc). This choice is a compromise between the known limitations (statistics and angular resolution) of the γ-ray data and the requirement to resolve variations in the inner Galaxy. The choice of the 4–8 kpc ring is based on our wish to separate the main concentration of molecular gas in the inner Galaxy.

The basic assumption characteristic of this method is that the γ-ray emissivity is a function of radius only; no attempt is made explicitly to resolve non-axisymmetric structure in the emissivity distribution (e.g. related to spiral arms) or to distinguish arm/interarm emissivity contrasts. However if contrasts are present, they will still be covered to some extent by the model via the $YW_{\mathrm{CO},i}$ term, since the CO is at least in part a tracer of spiral structure. In this case the value of Y derived from γ-rays will of course include the cosmic-ray contrast, and therefore be an overestimate of the true $N_{\mathrm{H_2}}/W_{\mathrm{CO}}$ ratio factor, which we denote by 'X'. The relation of Y to X is further discussed in Sect. 4.

Equation (1) is valid for each energy range separately, but we have to study also cases where all energy ranges are considered together, in order to investigate models with energy-independent parameters. For example we treat the case of energy-independent shape for $q(R)$ and energy independent Y by making fits to the three ranges simultaneously. The number of parameters to be determined then becomes quite large but the fitting routines are sufficiently robust to locate the maximum likelihood solution in about 20 iterations.

The inverse Compton emission was calculated using the model described in Strong (1985a). Although this estimate differs slightly from that used in Paper III, this has a small effect, and in any case the absolute level is determined via the free parameter f_{IC} derived from fits to the γ-ray data.

The four most intense γ-ray sources were explicitly included in the model via the final term. The sources are: the Vela pulsar, the Crab pulsar, Geminga (2CG195+4) and CG78+01. Note that the fluxes of these sources are free parameters, and in fact the resulting spectra are a useful by-product of this analysis.

The error analysis is performed using the information matrix technique described by Strong (1985b). The theoretical basis of the likelihood ratio method used is described in Paper III, and a detailed treatment can be found in Kendall and Stuart (1973), (Ch. 24). Here we use the notation: ΔN = number of parameters of model relative to the general model, $\Delta \ln L$ = log-likelihood of model relative to general model. Then $-2\Delta \ln L$ is distributed as $\chi^2_{\Delta N}$. We define $\mathscr{P}$ as the probability of obtaining a value of $-2\Delta \ln L$ greater than that observed, for a given model. The 'significance' is then $1-\mathscr{P}$. This method is a formally exact treatment of the statistical problem once the model has been defined. The 'general model' as given by Eq. (1) is found to be good enough to reproduce the observations as well as could be expected given the quality of the data, and so is probably sufficient for the purposes of the likelihood method, which requires that the 'general model' actually is the 'true' model for some particular set of values of the parameters (Kendall and Stuart, 1973, Ch. 23). Actually we may have rather more parameters than are strictly necessary to get a satisfactory fit; however this in no way affects the validity of the tests made with respect to this model.

The fits were done principally for $|b|<9.5°$ since the CO coverage is almost complete in this range. Since however the convolution means that coverage beyond this range is strictly necessary, most of the fits were also done with $|b|<5.5°$ to check for differences. In this range the coverage is complete for the convolution but the statistics and dynamical range are smaller. Additional runs with $10°<l<270°$ and $90°<l<350°$ were done to check for differences between the 1st and 4th quadrants.

3. Data

3.1. Gamma rays

The final COS-B database (Mayer-Hasselwander, 1985) contains a total of 65 observations, of which 55 include regions near

enough to the galactic plane to be of interest to be used in the present analysis. The baseline instrumental response as determined from pre-launch accelerator calibration is given by Mayer-Hasselwander (1985). The relative sensitivity of the instrument for these observations as well as the variations in background with time during the COS-B mission was determined by Strong et al. (1987). The method by which skymaps (consisting of counts and effective exposure) are constructed from the database is described by Strong et al. (1987). The maps used are those included with the final COS-B database. These assume an input spectrum of $E^{-1.85}$ for the exposure calculation; expected variations from this value have negligible effect on the exposure.

3.2. *H I surveys*

The 21-cm line surveys of Weaver and Williams (1973; $10° \lesssim l \lesssim 250°$) and Kerr et al. (1986; $240° \lesssim l \lesssim 350°$), and part of the survey of Strong et al. (1982b; $350° \lesssim l \lesssim 10°$), were used to obtain H I column densities for $|b| \lesssim 10°$. At $|b| \gtrsim 10°$, the survey of Heiles and Habing (1974) was used for the northern sky ($\delta \gtrsim -30°$) and that of Heiles and Clearly (1979) for the southern sky. The surveys were first corrected to obtain the brightness temperature and then column densities were derived assuming a uniform spin temperature of 125 K, as described in Papers I and II. The construction of column density maps for separate galacto-centric rings is described in Paper III.

Maps of the total H I column density from these data are shown in Fig. 1 (a), convolved with the COS-B point-spread function in the three energy ranges.

3.3. *CO surveys*

The CO ($J = 1$–0) data base used for our analysis is a composite of several surveys carried out over the last five years with the Columbia 1.2 m telescopes in New York City and on Cerro Tololo in Chile, and includes basically all the data in the large-scale panorama presented by Dame et al. (1987). The combined survey covers the entire galactic plane and is essentially complete up to $|b| \simeq 7°$ (particularly for the 1st and 4th galactic quadrants), with several large extensions to higher latitudes. The spatial resolution is 0.5°, The construction of velocity-integrated CO maps for separate galacto-centric rings is described in Paper III.

Maps of the integrated CO temperature are shown in Fig. 1 (b), convolved with the COS-B point-spread function in the three energy ranges.

4. Discussion of fitting results

Table 1 summarizes the fits performed, and Table 2 summarizes the resulting parameters, the log-likelihood values and the error estimates as determined from the information matrix. Table 3 gives the fitted intensities of the four point sources included in the model. In the following discussion the reader should refer to these tables for details. Note that the galactic centre region $350° < l < 10°$ was excluded in all fits, for the reasons discussed in Sect. 5.

4.1. *General*

A general statement can be made that, within the quoted uncertainties, the parameter values are consistent for different choices of the fitting region both in latitude ($|b| < 9.5°$ or $|b| < 5.5°$, cases 1 and 1b)) and longitude ($10° < l < 350°$, $10° < l < 270°$, $90° < l < 350°$, cases 1N and 1S).

A systematic effect can however be seen comparing the analysis using the separate regions (case 1N and 1S) with that for the total (case 1): the separate regions give a larger $q(R)$ gradient and a correspondingly lower Y value. This effect is most marked in the 70–150 MeV range, and may be related to the fact that when the separate regions are used, less weight is given to the inner Galaxy in the fits (which always include the whole $90° < l < 270°$ region). This effect is discussed later. It seems most natural to give equal weight to the inner and outer Galaxy and to use all the data together. Therefore in what follows we shall concentrate on the results from the total region ($|b| < 9.5°$, $10° < l < 350°$).

4.2. *Inverse Compton emission*

Since the estimate of this component is based on a model whose input (radiation fields and the cosmic ray electron spectrum) is subject to some uncertainty, it is necessary first to test whether our estimate is consistent with the data. Fits were made with f_{IC} free in each energy range, corresponding to the most general case of equation (1) (all parameters free). The result was in each case consistent with $f_{IC} = 1.0$ (0.65 ± 0.3, 1.6 ± 0.3, 1.1 ± 0.2 in the three energy ranges).

In the subsequent analysis the value was therefore fixed at $f_{IC} = 1.0$; the effect on the other parameters of the uncertainty in f_{IC} is negligible.

4.3. *Energy-dependent models*

We consider the models in order of increasing complexity, starting from the simplest, energy independent model. The statistical tests are made both against the most restricted (case 4) and the most general (case 1) model in each case, in order to test both whether the model is too complex or too simple considering the number of parameters involved, using the statistic explained in Sect. 2.

Note that testing the energy dependence of Y amounts to considering the possibility of different spectra for the γ-ray emission distributed like H I and that distributed like CO.

4.3.1. Test of case 4

In order to check for evidence that the model requires some energy dependence whether in the shape of the emissivity gradients or the value of Y, or both, we compare case 4 with 1. Then $\Delta \ln L = 11.5$, $\Delta N = 12$ and $\mathscr{P} = 0.03$. The energy dependence is less significant than found in Paper III, which may be due to a technical problem with the likelihood maximization in that paper. However, it is evident that the energy-independent model is too simple since it can be improved significantly by adding some energy dependence.

Figure 2 shows explicitly the likelihood as a function of Y for case 1; this is discussed later.

4.3.2. Tests of case 3

Relaxing the restriction that Y is energy independent, case 3 gives the next model in order of complexity.

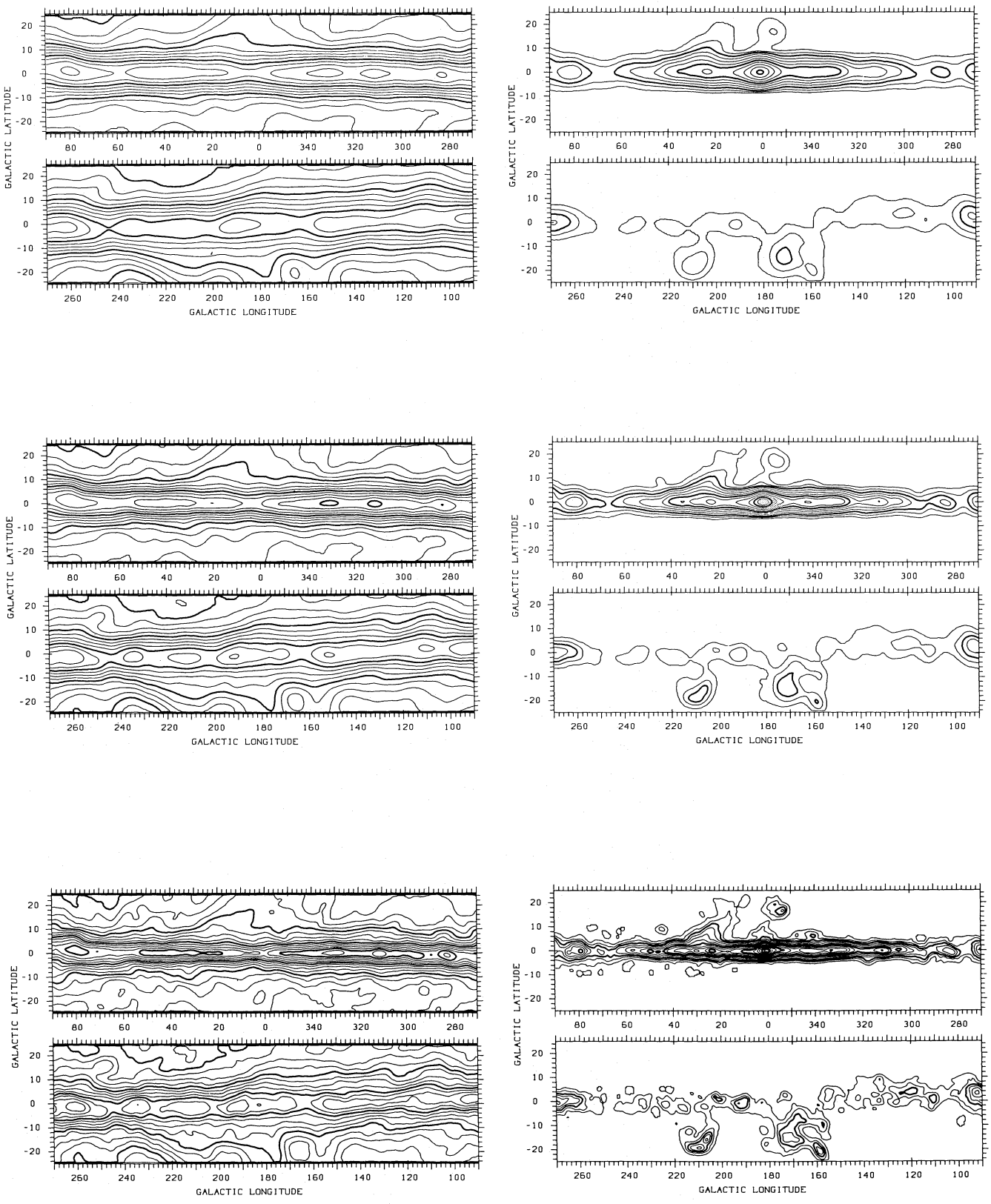

a b

Fig. 1a and b. Illustrations of gas data used: **a** H I total column density, contour interval: $5(10^{0.1n}-1)\,10^{20}$ atoms cm^{-2}. **b** CO integrated temperature contour interval: $5(10^{0.1n}-1)$ K km s^{-1}. Both maps are shown as convolved with the COS-B point-spread function in the three standard energy ranges used

Table 1. Summary of fits (blank entries indicate that the previous value applies)

Case	Longitude range (deg)	Latitude range (deg)	Gradient energy dependence	Y energy dependence	r	Number of parameters
1	10/350	−9.5/9.5	Dep.	Dep.	1.0	36
1b		−5.5/5.5				
1N	10/270	−9.5/9.5				
1S	90/350					
2	10/350	−9.5/9.5	Dep.	Ind.	1.0	34
2b		−5.5/5.5				
3	10/350	−9.5/9.5	Ind.	Dep.	1.0	26
3b		−5.5/5.5				
4	10/350	−9.5/9.5	Ind.	Ind.	1.0	24
4b	10/350	−5.5/5.5	Ind.	Ind.	1.0	24
1r	10/350	−9.5/9.5	Dep.	Dep.	0.5–3.0	37

We can test the energy dependence of Y by comparing case 3 with 4. Then $\Delta \ln L = 3.6$, $\Delta N = 2$ and $\mathscr{P} = 0.03$. There is therefore a weak indication of an energy dependence of Y from this test.

Since the shape of $q(R)$ remains energy independent in this case, comparing to the general model amounts to testing for energy dependence of $q(R)$. Comparing case 3 with 1, we have $\Delta \ln L = 8$, $\Delta N = 10$ and $\mathscr{P} = 0.1$. Hence there is barely an indication of an energy dependence in the shape of $q(R)$.

This model (case 3) is therefore both an improvement over the totally energy independent one, and not significantly worse than the general model.

4.3.3. Tests of case 2

The next model in order of increasing complexity comes from relaxing instead the condition of energy independent shape for $q(R)$, case 2.

We can test the energy dependence of $q(R)$ by comparing case 2 with 4. Then $\Delta \ln L = 3.3$, $\Delta N = 10$ and $\mathscr{P} = 0.8$. There is less evidence for an energy dependence than in the test of section 4.3.2. Since Y remains energy independent in this case, comparing to the general model amounts to testing for energy dependence of Y. Comparing case 2 with 1 we have $\Delta \ln L = 8.2$, $\Delta N = 2$ and $\mathscr{P} = 3\,10^{-4}$. Thus there is an indication for energy dependence of Y, but it should be noted that the effect is actually due to a difference between the ranges 70–150 MeV and >150 MeV.

The model studied in case 2 is therefore unsatisfactory by both criteria: it is not an improvement over the totally energy independent model, and is significantly worse than the general model. Note however that the cases 2 and 3 have practically the *same* value of $\ln L$, indicating that the fit is 'equally good' in the two cases. The difference in the significance of the energy dependent effects only arises from the different number of parameters in the two models.

The nature of the low energy Y value is further studied in Sect. 4.6, where radial variations of this parameter are considered.

4.3.4. The 'best' model

From the results of the tests described above, case 3 is the only one which is both an improvement on the simple energy independent model and not significantly worse than the most general model. It thus qualifies for the classification 'best' model. As mentioned above, the energy dependence in this model is actually due to a difference in Y between the ranges 70–150 MeV and >150 MeV: $Y(70\text{–}150\ \text{MeV}) = (3.3 \pm 0.5)\ 10^{20}$ molecules cm^{-2} (K km s^{-1})$^{-1}$ and $Y(>150\ \text{MeV}) = (2.5 \pm 0.3)\ 10^{20}$ molecules cm^{-2} (K km s^{-1})$^{-1}$. It is gratifying that this 'best' model is actually rather simple, with the same shape of $q(R)$ in each energy range, and all the energy dependence in the parameter Y. However the systematic effect discussed in Sect. 4.1 remains a worry; we return to this problem in Sects. 4.6 and 4.7 where the nature of the low-energy Y value is discussed further.

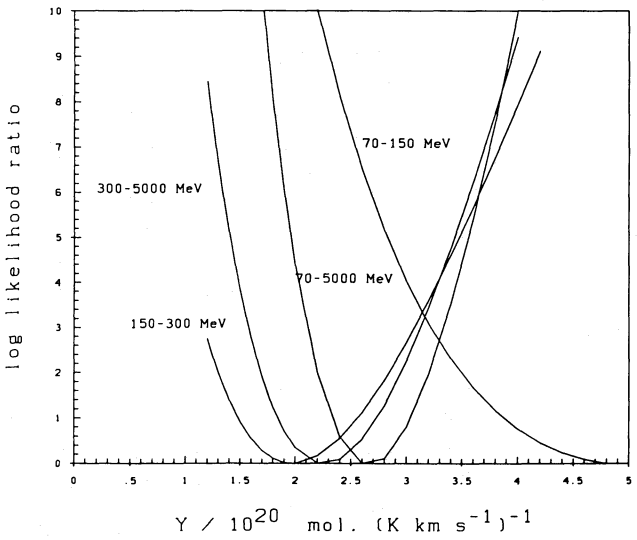

Fig. 2. Log-likelihood ratio as function of Y for the three energy ranges, and for the three ranges summed. The model and data correspond to case 1

4.4. The value of the CO-to-H_2 conversion factor

The choice of a 'best' value for the 'physical' conversion factor from CO integrated temperature to H_2 column density must depend on how we choose to treat the fact that the fitted value of Y in equation (1) is larger at low energies (cf. case 3). Since X is by

Table 2a. Results of fits: parameters and log-likelihood values

Case	q_1	q_2	q_3	q_4	q_5	q_6	I_B^0	Y	$-\ln L$	$-\sum \ln L$
70–150 MeV										
1	0.98	0.87	0.96	0.71	0.84	0.83	6.39	5.01	13182.2	38008.8
1b	1.08	1.03	1.05	0.77	1.07	1.11	5.30	4.38	8097.3	23772.2
1N	2.12	1.35	1.12	0.89	0.96	0.80	6.04	3.22	10131.6	
1S	1.82	1.12	1.23	0.93	1.08	0.90	5.67	2.93	9642.4	
2	1.62	1.45	1.23	0.97	1.06	0.75	5.86	2.60		38017.0
2b	1.53	1.46	1.25	0.96	1.29	1.08	4.79	2.80		23775.5
3	1.39	1.26	1.11	0.94	0.83	0.70	6.15	3.30		38016.7
3b	1.40	1.34	1.16	1.02	0.90	0.80	5.56	3.12		23779.9
4	1.60	1.40	1.23	1.04	0.93	0.79	5.74	2.70		38020.3
4b	1.55	1.47	1.27	1.11	0.99	0.89	5.06	2.70		23781.0
1r	1.72	1.29	0.91	0.67	0.80	0.85	6.44	5.50	13186.8[a]	
	0.54	0.54	1.00	0.73	0.86	0.82	6.35	4.67	13179.4[b]	
150–300 MeV										
1	1.28	0.92	0.74	0.60	0.59	0.42	2.60	1.97	12433.8	
1b	1.07	0.79	0.69	0.56	0.61	0.44	2.64	2.45	7838.6	
1N	2.28	1.17	0.84	0.68	0.67	0.41	2.37	1.41	9538.9	
1S	3.60	1.36	0.81	0.75	0.70	0.43	2.29	0.46	9040.4	
2	1.07	0.76	0.68	0.54	0.56	0.43	2.73	2.60		
2b	0.98	0.72	0.66	0.52	0.58	0.44	2.74	2.80		
3	0.88	0.79	0.70	0.59	0.52	0.44	2.64	2.51		
3b	0.81	0.78	0.67	0.59	0.52	0.46	2.61	2.66		
4	0.86	0.76	0.66	0.56	0.50	0.43	2.71	2.70		
4b	0.81	0.76	0.66	0.58	0.51	0.46	2.62	2.70		
1r	1.97	1.20	0.71	0.59	0.59	0.43	2.61	2.15	12433.2[a]	
300–5000 MeV										
1	0.77	0.81	0.66	0.63	0.43	0.40	2.22	2.25	12392.7	
1b	0.71	0.84	0.66	0.66	0.42	0.41	2.11	2.22	7836.3	
1N	0.00	0.87	0.67	0.64	0.42	0.40	2.19	2.22	9575.2	
1S	1.37	0.91	0.70	0.68	0.46	0.40	2.08	1.68	9048.5	
2	0.69	0.74	0.63	0.59	0.41	0.40	2.29	2.60		
2b	0.59	0.71	0.61	0.60	0.38	0.41	2.29	2.80		
3	0.83	0.76	0.67	0.56	0.50	0.42	2.28	2.44		
3b	0.78	0.75	0.65	0.57	0.50	0.45	2.14	2.48		
4	0.82	0.71	0.63	0.53	0.47	0.40	2.37	2.70		
4b	0.76	0.72	0.62	0.54	0.49	0.44	2.26	2.70		
1r	1.29	1.08	0.64	0.62	0.42	0.40	2.22	2.44	12394.1[a]	

Notes to Table 2:
[a] In this fit the value of r was fixed at 0.5, and the value of Y is that for $R > 8$ kpc
[b] In this fit the value of r was fixed at 2.0, and the value of Y is that for $R > 8$ kpc
$f_{ICS} = 1.0$ in all fits shown here.
Units: q_i: 10^{-26} atom^{-1} sr^{-1} s^{-1}, I_B^0: 10^{-5} cm^{-2} sr^{-1} s^{-1}, Y: 10^{20} molecules cm^{-2} (K km s^{-1})$^{-1}$.
$\sum \ln L$ refers to the summed likelihood over the three energy ranges.

definition energy-independent, there are (at least) four possible situations:

(i) systematic effects due to the poor angular resolution for 70–150 MeV

(ii) other components (e.g. sources) with steep spectra which also correlate with the CO distribution

(iii) effects related to cosmic-ray propagation or production in molecular clouds

(iv) energy-dependent spiral arm/interam cosmic-ray contrasts

In each case it is clear that the value of Y in the low energy range is the least reliable indicator of X. The value also depends slightly on whether we assume an energy independent shape for $q(R)$ or not. Our best estimate is made using cases 1 and 3 for the 150–300 and 300–5000 MeV ranges; the value of Y ranges from 2.0 to 2.5 10^{20} molecules cm^{-2}(K km s^{-1})$^{-1}$, so we adopt $X = 2.3 \pm 0.3\ 10^{20}$ molecules cm^{-2}(K km s^{-1})$^{-1}$.

However, it should be kept in mind that this value is an upper limit if a population of unresolved γ-ray point sources exists with an angular distribution similar to that of the molecular gas, or if

Table 2b. Results of fits: error estimates for parameters (errors are for 1σ)

Case	q_1	q_2	q_3	q_4	q_5	q_6	I_B^0	Y
70–150 MeV								
1	0.28	0.14	0.09	0.10	0.20	0.16	0.25	0.92
1b	0.35	0.20	0.11	0.13	0.26	0.21	0.53	0.92
1N	0.85	0.26	0.11	0.13	0.23	0.17	0.29	0.71
1S	0.67	0.23	0.13	0.15	0.23	0.18	0.33	0.88
2	0.42	0.07	0.05	0.09	0.21	0.17	0.21	0.25
2b	0.42	0.07	0.06	0.11	0.25	0.22	0.46	0.32
3		no	error	analysis			0.28	0.47
3b							0.54	0.58
4							0.26	0.33
4b							0.50	0.45
1r	0.47	0.18	0.09	0.10	0.19	0.16	0.26	0.99
	0.16	0.10	0.09	0.10	0.20	0.17	0.25	0.85
150–300 MeV								
1	0.33	0.11	0.04	0.06	0.11	0.08	0.13	0.38
1b	0.31	0.13	0.06	0.07	0.12	0.10	0.26	0.55
1N	0.99	0.16	0.06	0.06	0.11	0.08	0.15	0.34
1S	1.14	0.24	0.06	0.08	0.12	0.09	0.17	0.35
2	0.24	0.04	0.02	0.04	0.10	0.08	0.10	0.25
2b	0.23	0.04	0.03	0.05	0.11	0.09	0.21	0.32
3		no	error	analysis			0.14	0.33
3b							0.27	0.43
4							0.15	0.37
4b							0.27	0.45
1r	0.45	0.11	0.04	0.06	0.11	0.08	0.13	0.39
300–5000 MeV								
1	0.25	0.08	0.04	0.05	0.09	0.06	0.11	0.31
1b	0.26	0.10	0.04	0.06	0.09	0.08	0.21	0.37
1N	0.64	0.10	0.04	0.05	0.09	0.06	0.12	0.35
1S	0.41	0.12	0.05	0.06	0.09	0.07	0.14	0.38
2	0.21	0.03	0.02	0.04	0.08	0.06	0.09	0.25
2b	0.20	0.03	0.02	0.04	0.09	0.08	0.16	0.32
3		no	error	analysis			0.11	0.28
3b							0.21	0.35
4							0.12	0.33
4b							0.22	0.42
1r	0.35	0.12	0.04	0.05	0.08	0.06	0.11	0.33

Table 3. Results of fits: spectra of point sources

Energy range	Source			
	CG78+1	Crab	Geminga	Vela
70–150 MeV	1.15 ± 0.38	4.8 ± 0.45	2.63 ± 0.4	7.72 ± 0.61
150–300 MeV	0.76 ± 0.16	1.27 ± 0.17	1.29 ± 0.16	4.06 ± 0.29
300–5000 MeV	0.55 ± 0.11	0.82 ± 0.12	1.59 ± 0.15	4.59 ± 0.26

Units: 10^{-6} photons $cm^{-2}\ s^{-1}$

the cosmic-ray density is enhanced in molecular clouds. (Such an effect would be expected e.g. in the model of Bignami and Fichtel (1974) in which cosmic-ray enhancements are associated with spiral arms).

A detailed discussion on the application of X and a comparison with other determinations is given by Bloemen et al. (1986).

4.5. *Radial dependence of emissivity*

All the results in Table 2 show that $q(R)$ is relatively insensitive to the choice of data or model, the differences being within the quoted error bars. Figure 3a shows $q(R)$ in each energy range in

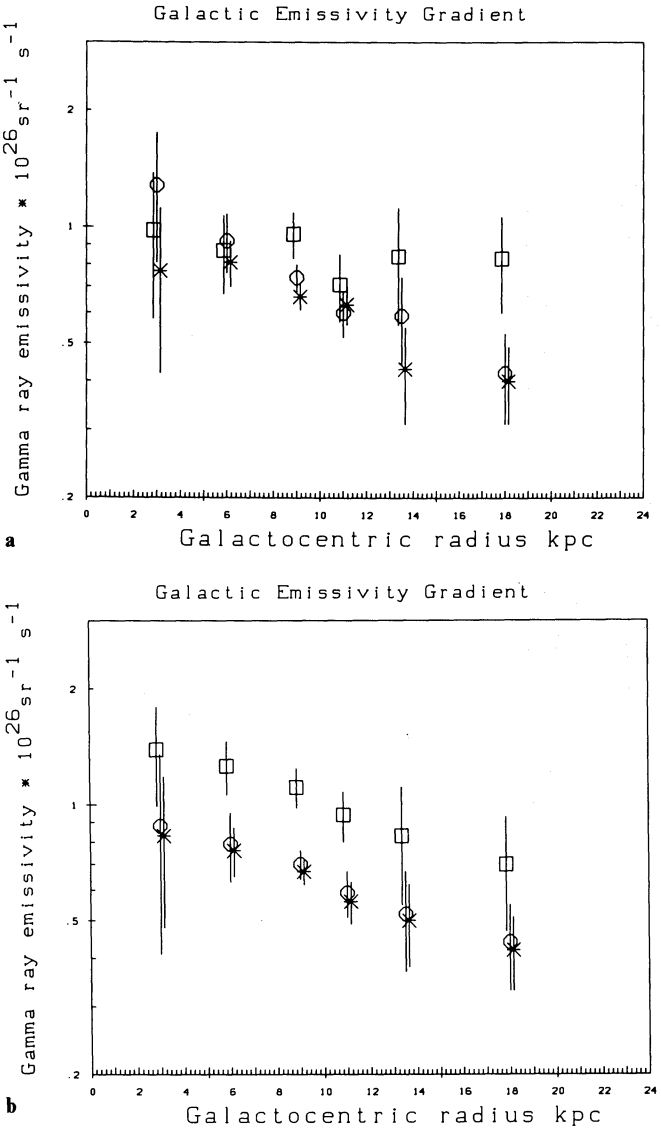

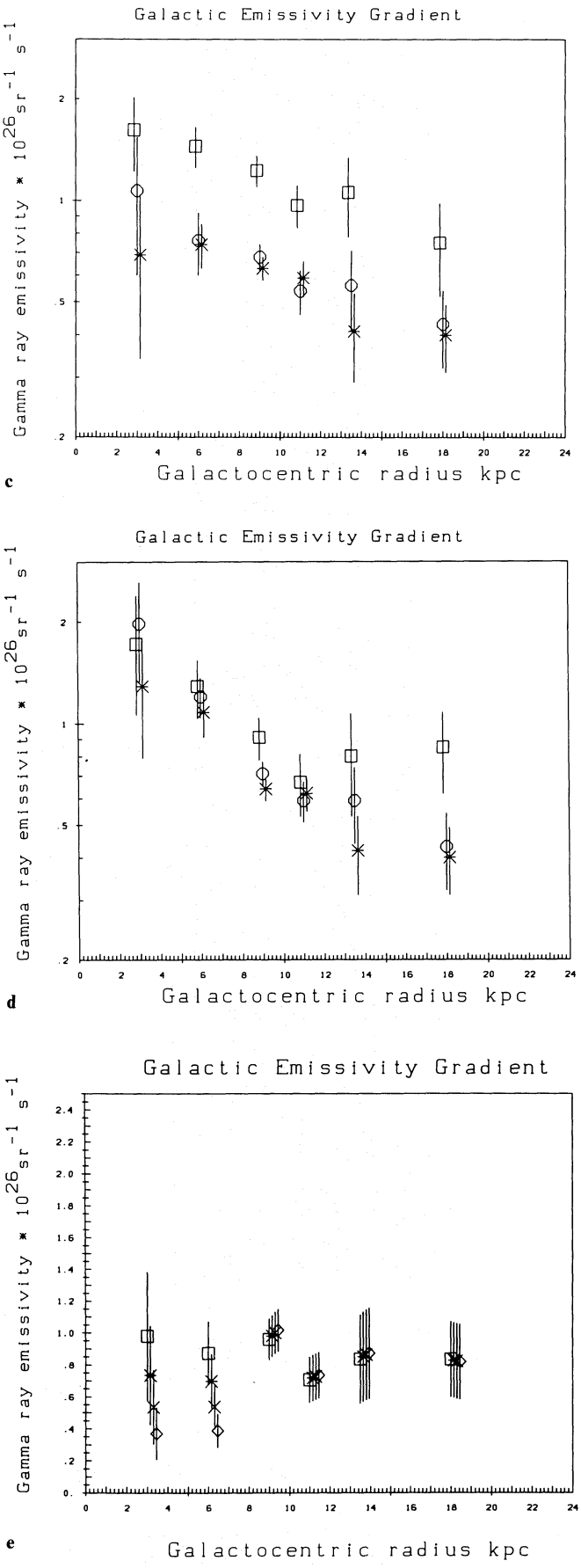

Fig. 3a–e. Radial distribution of γ-ray emissivity: **a** for $q(R)$ shape and Y energy dependent (case 1); **b** for $q(R)$ shape energy independent, Y energy dependent (case 3); **c** for $q(R)$ shape free, Y energy independent (case 2); **d** for $r=0.5$ (case 1r). Energy ranges indicated by symbols: squares: 70–150 MeV, circles: 150–300 MeV, stars: 300–5000 MeV. **e** for $1.0<r<3.0$ and 70–150 MeV. Squares: $r=1.0$, stars: $r=1.4$, crosses: $r=2.0$, diamonds: $r=3.0$

the case of gradient and Y energy dependent (case 1).[1] The radial variation is small as found in Paper III, amounting to at most a factor 2 between the inner and outer Galaxy, and 1.5 between the inner Galaxy and the solar circle.

Figure 3b shows $q(R)$ in the case of an energy independent shape (case 3), which is consistent with the data as shown previously. Comparing with Fig. 3a the differences are within the quoted errors for each case. The main difference is in the inner Galaxy at low energies (see the discussion in Sect. 4.6). Figure 3c shows $q(R)$ for the case of a free shape with energy-independent Y(case 2). Again the main difference is in the inner Galaxy at low energies.

The effect on $q(R)$ of possible variations of Y with radius are considered in the next section.

4.6. *Radial variation of Y*

In the models discussed so far, Y has been assumed independent of galactocentric radius. Since this is not necessarily true, and indeed claims of substantial variation have been made together with the suggestion that this has a large effect on $q(R)$ (Bhat et al. 1985a, b), we explicitly test the variation of Y with R against the γ-ray data. We define

$$r = Y(2-8\,\mathrm{kpc})/Y(>8\,\mathrm{kpc})$$

and repeat the fits for a range of values of r (case 1r). Figure 4 shows $L(r)$ for the 3 energy ranges and for the >150 MeV range. This figure shows that the data above 150 MeV are consistent with $r=1.0$ (no variation of Y with R). Since in the low energy range Y is not a good indicator of X, we use the two higher ranges to determine the formal limits on r: $r=0.8\pm0.2$. Further using these ranges we find that $\Delta \ln L\,(r=0.5)=1.5$, corresponding to $\mathscr{P}=0.08$ (1 degree of freedom) so that a factor 2 variation in Y is improbable but not excluded.

Although this argues against an X variation as large as that adopted by Bhat et al. (1985a, b) we show in Fig. 3d the corresponding $q(R)$ for $r=0.5$. The gradient is only slightly larger than for $r=1.0$, the difference being limited by the fact that the H I component is not affected by the X value. We conclude that variations of X in the Galaxy, even if present, do not have a major influence on our derived emissivity gradients. This may be important since the existence of a factor 2 increase in the O/H ratio in the inner Galaxy has recently been clearly established by IR emission-line observations (Lester et al., 1987), although CO intensity may not scale with CO abundance (see Kutner and Leung, 1985; Solomon et al., 1987).

The 70–150 MeV case is somewhat different, Fig. 4 showing a clear indication for $r>1$. (The likelihood value actually continues slowly to increase asymptotically as Y increases.)[2] The formal significance is given by $\Delta \ln L=4.8$ with $\Delta N=1$, giving $\mathscr{P}=2\,10^{-3}$.

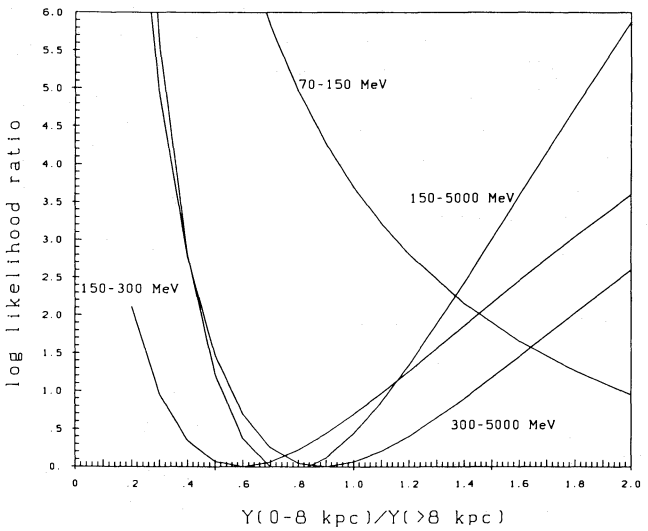

Fig. 4. Log-likelihood as a function of the ratio $r=Y(2-8\mathrm{kpc})/Y(>8\mathrm{kpc})$ for each energy range (case 1r)

This means that in the inner rings essentially all the emission is attributed to the CO-like component. To illustrate this, Fig. 3 (e) shows $q(R)$ for the range $1.0<r<3.0$, which is roughly the range of uncertainty in r. As r increases, there is a decrease in the corresponding $q(R)$ in the inner Galaxy. The uncertainty in $q(2-4$ kpc) and $q(4-8$ kpc) is clearly very large; the reason for this is the difficulty in distinguishing the structures of the H I and CO in the data after convolution with the wide 70–150 MeV COS-B point-spread-function, which is somewhat uncertain in this energy range. Specifically, the inner Galactic disk (inside $R=8$ kpc) is not resolved below 150 MeV, so that the thickness of the predicted disk is sensitive to the adopted PSF width. A CO disk about 1° thick convolved with a 3°.5 wide PSF has the same apparent thickness as a 2° wide H I disk convolved with a 3°.0 wide PSF. While the sum of the H I and CO contributions is strongly constrained by the data, their ratio is highly uncertain in the inner Galaxy at low energy. As long as the structures are resolved (as is the case outside 8 kpc for 70–150 MeV and everywhere at higher energies) the problem is minimized.

Also note that for $r>1.2$, $q(R)$ *increases* with R in the inner Galaxy for 70–150 MeV; although not impossible *a priori* it does seem very unlikely that such a sharp change in behaviour with respect to the higher energy ranges occurs. If we insist that $q(R)$ does not increase with R, then we find that $r<1.2$, i.e., consistent with higher energies. We therefore adopt the assumption that $r=1.0$ in drawing conclusions in this paper.

Under this assumption we are left with the conclusion that Y is larger in the 70–150 MeV range. The preferred model is then case 3 (shape of $q(R)$ energy independent), with Y(70–150 MeV) $=3.3\pm0.5\,10^{20}$ molecules cm^{-2}(K km s^{-1})$^{-1}$.

4.7. *Again, the 'best' model*

Although we are still left with the conclusion that case 3 (with $r=1.0$) is the preferred model after the test in the previous section, we have lost some confidence in this model. The reason is the finding in Sect. 4.6 of a formally high significance for an effect (an increase in $q(R)$ with R for 70–150 MeV) which can almost certainly be excluded on physical grounds. This may indicate an

[1] Error bars in Fig. 3 are shown for $\Delta \ln L=1.0$, corresponding to 1.4σ. Also, Figs 3a–c all use errors from Case 1, since this reflects better the full uncertainty.

[2] The effect is evidently related to the energy dependence of Y found in Sect. 4.3.3. This effect was already evident in the fits using the 1st and 4th quadrants separately (Sect. 4.1), where more weight is given to the anticentre and the average Y value appears smaller than when these quadrants are both included in the fit.

incompleteness of the model for the low energy range, but it is hard to improve on it because of the wide COS-B point-spread function in this range. Another indication of the same problem is the systematic difference (see Sect. 4.1) between the fits using the 1st and 4th quadrants separately and the fit including both quadrants. In summary: although our tests indicate that an energy-dependent Y is preferred to an energy-dependent shape of $q(R)$, we have indications that the energy dependence may in fact be due to another effect not encompassed by our model.

5. Comparison of model with the observations

It is neither possible nor desirable to show the comparison of the data with each of the model fits listed in Table 2, so the 'best' model (in the sense of Sect. 4.3.4) is chosen, corresponding to an energy independent shape of $q(R)$ (case 3).

Figure 5 shows longitude distributions for $|b|<5°.5$. The four fitted point sources are included in the plot. In this presentation the other cases appear almost indistinguishable from this one. Considering that systematic uncertainties in exposure can lead to fluctuations of up to 10% on top of the statistical noise, the fits are generally quite satisfactory, and show that the model is adequate to account for the bulk of the diffuse emission along the entire galactic plane.

Towards the inner Galaxy, $|l|<60°$, H I and H_2 produce approximately equal contributions to the γ-ray intensity, indicating approximate equality of the mass in these components.

Arm-interam contrasts in emissivity are not explicitly included in our fit, and there is no indication that they are required by the data. However note that to some extent the model can adjust to such contrasts via the Y term, since the CO is at least in part a tracer of spiral structure.

Despite the general good agreement there are some significant deviations deserving attention. Most prominent is the galactic centre region, $|l|<10°$, which is well known to deviate strongly from the behaviour along the rest of the galactic plane (Blitz et al., 1985; Bania, 1986; Stacy et al., 1987), and which was not included in the present fits for this reason. Stacy et al. (1987) have recently shown that this discrepancy may be accounted for by wide-line molecular clouds in the vicinity of the galactic centre.

Also prominent are the excesses in $330°<l<345°$ for >300 MeV. These are approximately coincident with the positions of the sources 2CG333 and 2CG342 (Swanenburg et al. 1981). There are corresponding peaks at lower energies, but they are much less evident in the longitude plots, consistent with the hard spectrum found by Swanenburg et al. Also noticeable is the excess around 2CG235+1 and in the Carina region ($280°<l<290°$). A significant dip visible at all energies around $60°<l<70°$ corresponds to a well-known interarm region and may be the only hint in favour of an arm-interarm emissivity contrast.

Figure 6 shows latitude profiles of predicted and observed γ-rays for the inner ($300°<l<60°$) and outer ($60°<l<300°$) Galaxy. The agreement is satisfactory, except that there seems to be an excess relative to the model for $|b|>10°$ (this latitude range was not included in the fits).

6. Comparison with local emissivities from intermediate latitudes

The average emissivity in the distance range $8<R<12$ kpc from the present work can be compared with the independent estimates of the local value within a few hundred parsecs using γ-ray, galaxy count and gas data at intermediate latitudes ($10°<|b|<20°$). Strong et al. (1985) derived the values (1.10 ± 0.14, 0.76 ± 0.09, 0.68 ± 0.09) 10^{-26} sr^{-1} s^{-1} for the same three energy ranges as used here. By comparison the present values for $8<R<12$ kpc are, taking case 3 as representative, (1.02 ± 0.10, 0.65 ± 0.06, 0.62 ± 0.06) in the same units. The agreement (within the quoted errors) is remarkable given the very different latitude range and survey data used, and known problems with the galaxy counts calibration (see Lebrun, 1986).

7. The mass of molecular hydrogen in the inner Galaxy

As noted in Sect. 5, Fig. 5 shows that the contributions to the γ-ray emission from H I and H_2 are about equal in the inner Galaxy, and this immediately leads to $M_{H_2}\sim M_{H\,I}$. Henderson et al. (1982) find $M_{H\,I}=0.9\,10^9\,M_\odot$ in the inner Galaxy.

In Paper III the value for the total mass of the molecular hydrogen in the inner Galaxy (2–10 kpc) was found to be $\sim 10^9\,M_\odot$; this assumed however that the first and fourth quadrants are fully symmetric. Bronfman et al. (1988) did not make this assumption and derived $1.2\,10^9\,M_\odot$ from a combination of the Northern and Southern hemisphere Columbia data and applying the X-value obtained in Paper III. Scaling to the X-value obtained here gives $1.0\,10^9\,M_\odot$. Again, for the reasons mentioned in Sect. 4.4, this value should in fact be regarded as an upper limit. Further discussion on this point and a comparison with previous determinations is given by Bloemen et al. (1986).

8. Comparison with Papers I–III

Since this is the fourth paper in a series addressing the same general theme, it is important to point out and resolve any differences in conclusions between this and earlier papers. Papers I and II were concerned only with the outer Galaxy and longitudes $90°<l<270°$, and used only total H I column densities. Paper I concluded that the emissivity gradient is undetectable in the outer Galaxy above 300 MeV, but significant for 70–150 MeV. Paper II came to a similar conclusion using three galactocentric rings (10–12, 12–15 and >15 kpc). The present work confirms the small gradient at high energy, but finds no detectable energy dependence of the gradient, even in the outer Galaxy. Reference to Paper I shows that the conclusion was based on a local value for q(70–150 MeV) from early γ-ray-Galaxy count correlation studies (Strong et al., 1982a); subsequent analyses have reduced the local q-value, so that the anticentre gradient is correspondingly reduced, and is consistent with the present paper. In Paper II the effect found was not extremely significant, and the limits on the gradient are fully consistent with the present analysis. In any case the neglect of molecular hydrogen in Papers I and II means that these analyses are superseded by the present one.

In Paper III the first three galactic quadrants and the Carina region were used, and the analysis principle was the same as in this paper. It was concluded that Y is energy-independent to within the accuracy of the analysis, while the shape of $q(R)$ was found to depend on energy. This was then interpreted as a steeper gradient for cosmic-ray electrons compared to nuclei. The present paper confirms the small gradient at high energies, but ascribes the energy-dependence instead of to the Y-value, although there may be some incompleteness in our model (Sect. 4.7).

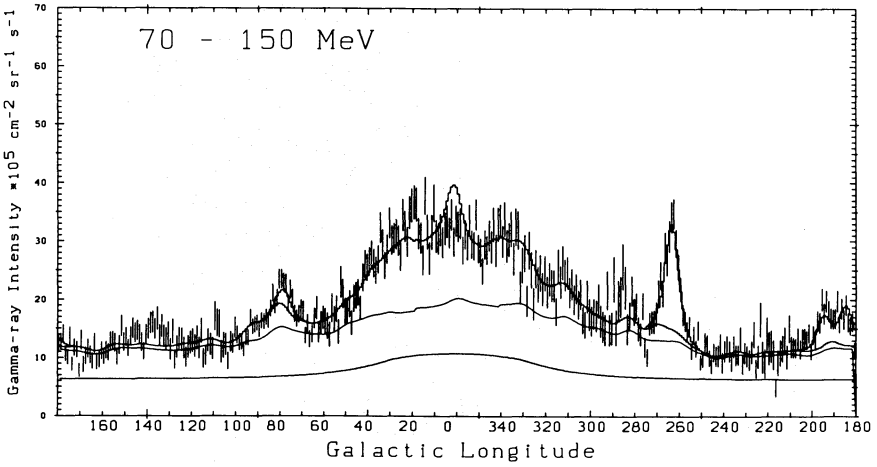

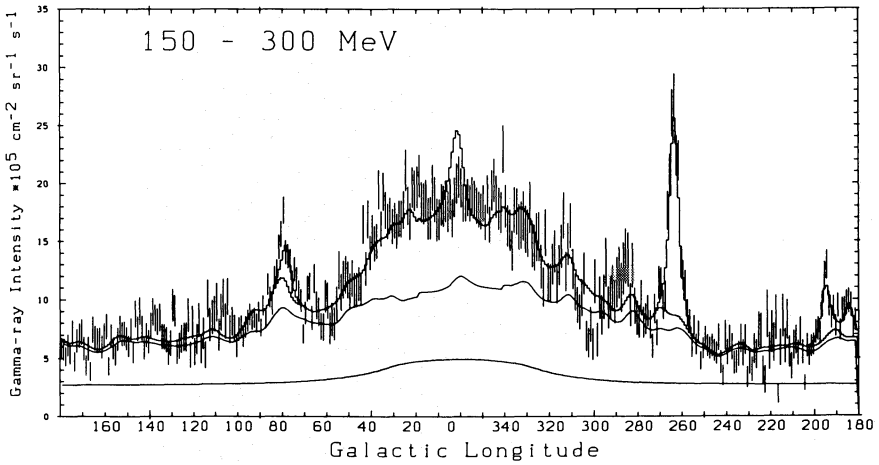

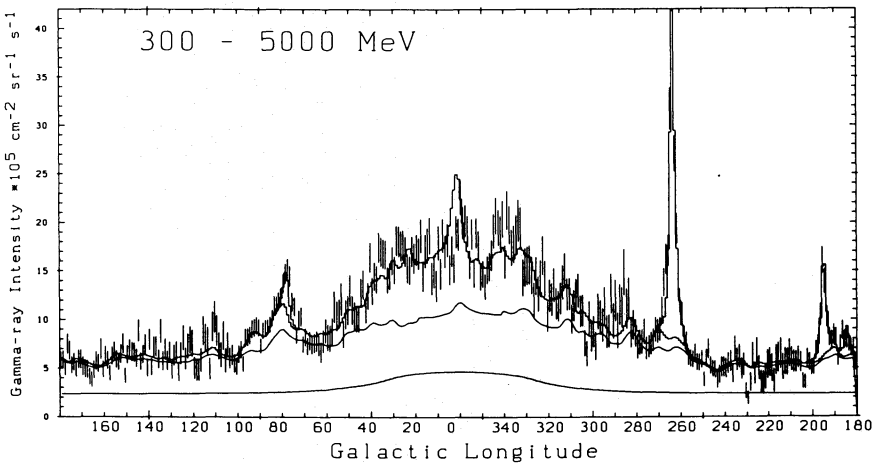

Fig. 5. Longitude distributions of predicted and observed γ-ray intensity, averaged over $|b| < 5.5°$. The model corresponds to energy independent shape of emissivity gradients (case 3), but appears almost identical in this presentation for the other cases. Vertical bars: γ-ray intensities measured by COS-B: $\pm 1\sigma$ error bars. Continuous lines: predicted γ-ray intensities as follows: lower line: inverse Compton emission, middle line: emission from H I, upper line: total model, including H I, H_2, inverse Compton and four point sources. All predictions include the fitted isotropic background (celestial + instrumental)

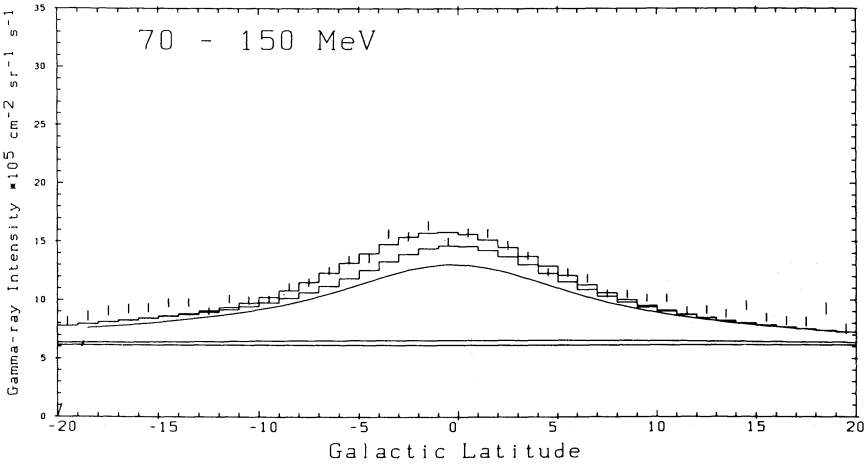

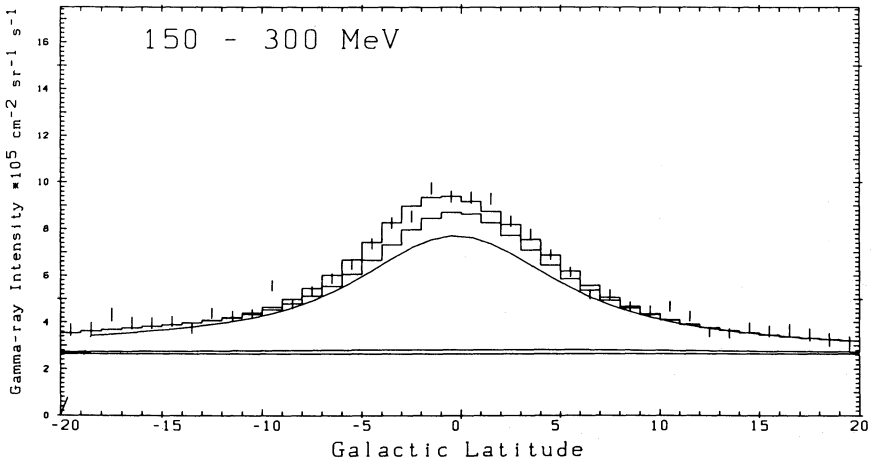

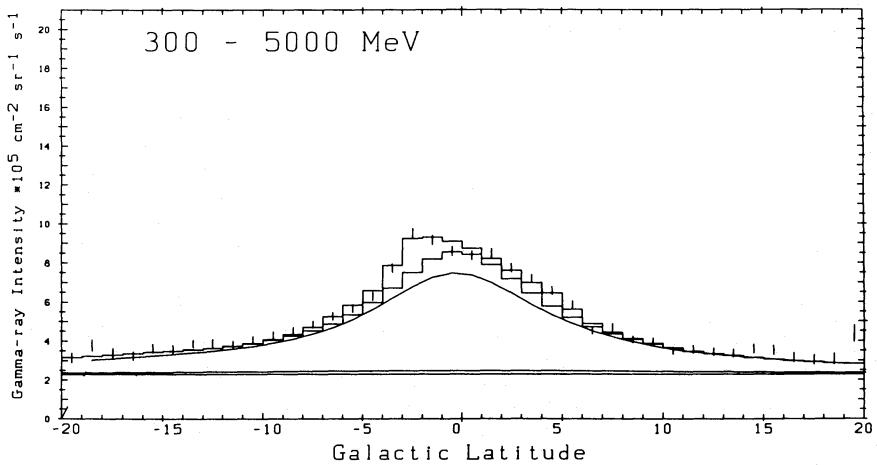

a

Fig. 6a and b. Latitude distributions of predicted and observed γ-ray intensity. **a** $300° < l < 60°$, omitting $350° < l < 10°$. **b** $60° < l < 300°$. Predictions as described in the caption to Fig. 5

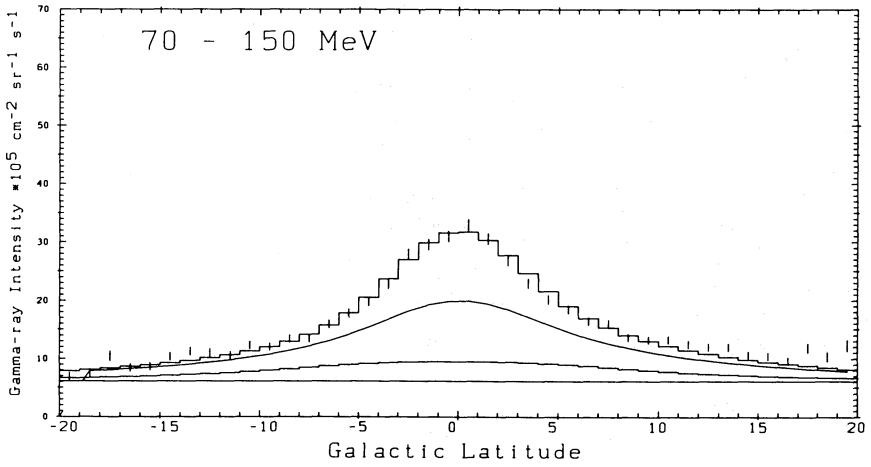

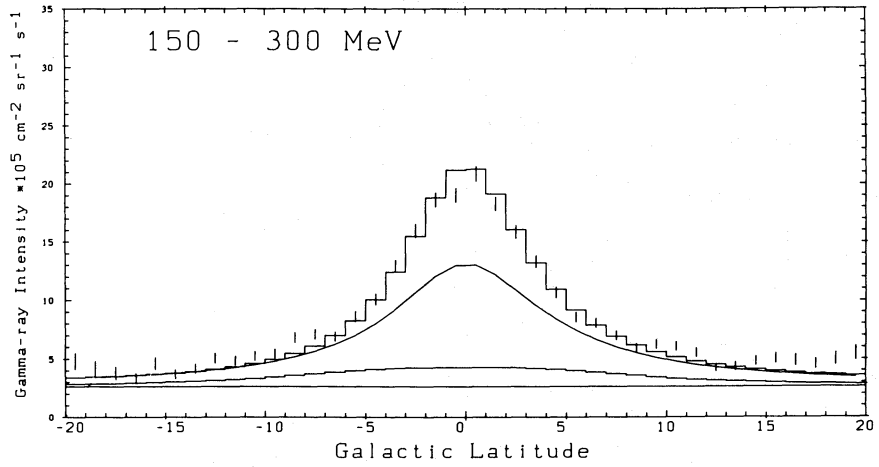

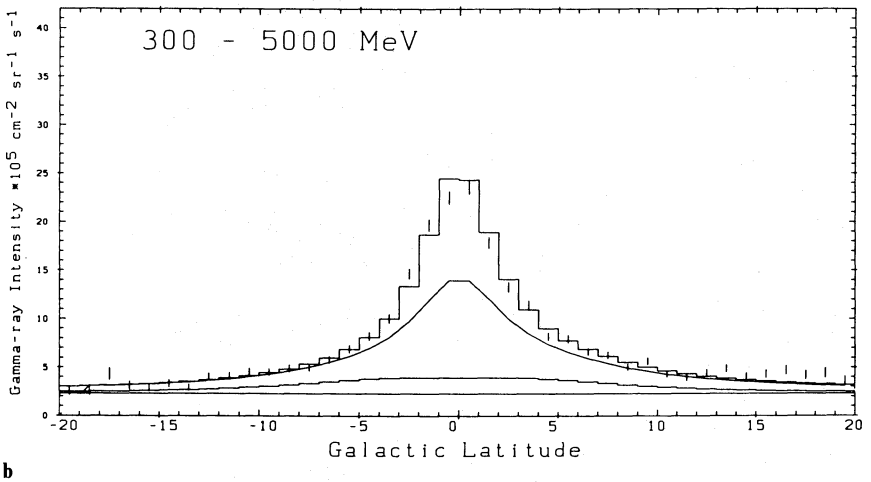

b

Fig. 6b

There are therefore some differences in the conclusions of Papers III and IV which require comment. In Paper III the evidence for the energy-dependent gradient was not overwhelming, and the energy-dependent Y was stated as also acceptable. There is therefore no real inconsistency between the two analyses; the better data and treatment has simply produced a more reliable result. The improvements include the extension of the CO surveys to include the entire southern Galaxy, as well as extensive upgrading and filling-in for many other regions. Also, the final COS-B database with its additional observations and final corrections has been used. Further, the analysis has improved technically with fully automated minimization and error calculation for the very many parameters involved.

For all these reasons, we regard the present analysis being the most reliable up to the present time.

9. Comparison with other results

9.1. The 'Durham' analyses

The Durham group have published many results on the topic studied here (e.g. Bhat et al., 1985a, b, 1986). Although their findings are not drastically different from ours, there is some discrepancy, at least in the conclusions. This is largely a result of the difference in philosophy between our approach and that of the Durham group. We determine Y and $q(R)$ simultaneously from the large-scale γ-ray-gas correlation study (via the different spatial structures of H I and CO in selected galactic rings) whereas the Durham group generally uses non-γ-ray estimates of X and then sets $Y=X$ in order to determine $q(R)$. A detailed comparison of the methods is given by Bloemen (1988).

They find a lower Y value for some local clouds, and this was considered as support for their independent (non-γ-ray) estimates. The most recent value derived by this group (Bhat et al., 1986) is $X=1.5\,10^{20}$ molecules cm^{-2}(K km s^{-1})$^{-1}$ locally, falling with decreasing R. Their local value is thus barely consistent with ours; further, their implied inner Galaxy value of $0.8\,10^{20}$ molecules cm^{-2} (K km s^{-1})$^{-1}$ is inconsistent with our value discussed in Sect. 4.4 (see Fig. 2), even considering our case where Y is a function of R. Note however that when in a later work (Szabelski et al., 1987) they *use* as input to a γ-ray analysis a value of $2.0\,10^{20}$ molecules cm^{-2} (K km s^{-1})$^{-1}$, which is consistent with our value, this leads to emissivity gradients similar to ours.

9.2. The 'Great Ring'

The emissivity gradients derived here can be compared with the results of Harding and Stecker (1985). They claim a large peak in $q(R)$ for $3.5<R<5.5$ kpc for the 4th quadrant, based on COS-B data >100 MeV and >300 MeV. Figure 5 shows however that we get an excellent fit to the data >150 MeV with *no such peak* in $q(R)$. The large peak found by Harding and Stecker appears to originate from the effect on their unfolding procedure of the sharp edge in the longitudinal γ-ray distribution at $l=330°$, which is due at least in part to discrete sources in this region as described in Sect. 5. The fact that the excess in this region is not present in the two lower energy ranges argues against attributing it to enhanced emissivity in the '5 kpc ring'. The result of Harding and Stecker may be attributed to their use of integrated $|b|<10°$ γ-ray profiles without considering the latitude information, and the absence of a treatment of the instrumental resolution in their analysis.

10. Conclusions

The diffuse galactic γ-ray emission in the range 70–5000 MeV is well represented by the sum of contributions from atomic and molecular hydrogen with a small inverse-Compton component. The required emissivity gradient is small, with a maximum variation from the solar circle to the inner Galaxy of a factor 2. The gradient is much smaller than that of the distribution of supernova remnants or pulsars. Therefore the arguments sometimes made invoking the γ-ray gradient as direct support for cosmic-ray origin in such objects cannot be substantiated; cosmic-ray propagation effects have to be taken into account.

Our 'best model' is one in which Y is energy dependent, while the shape of the emissivity variation is energy independent. The steeper γ-ray spectrum towards the inner Galaxy is then accounted for by a Y-value increasing at low energies by about 40%. Although an energy dependent emissivity variation can also fit the data, our statistical tests indicate that it is less satisfactory when the number of degrees of freedom are taken into account. The energy dependence of Y leads us to doubt the reliability of Y as a measure of X in the 70–150 MeV range, and hence we use the fits for >150 MeV for our 'best value' of X: $2.3\pm0.3\,10^{20}$ molecules cm^{-2}(K km s^{-1})$^{-1}$. This leads to an estimate for the mass of molecular hydrogen in the inner Galaxy of $1.0\,10^{9}$ $M_\odot$ in good agreement with our previous estimates and now based on the CO surveys of both the northern and southern Galaxy.

The energy dependence of Y is an interesting result perhaps related to physical processes associated with cosmic-ray propagation in molecular clouds, such as production of secondary electrons. Alternatively, steep-spectrum γ-ray sources spatially correlated with clouds would give a similar effect.

Finally, it can be noted that the energy-dependence of Y may be an artifact if our model is incomplete. In particular, cosmic-ray spectral variations as a function of distance from the galactic plane are not included in our model and would have a complicating effect. Indications for such variations have been found in independent studies of the COS-B data and radio-continuum data at 408 and 1420 MHz (Reich and Reich, 1988; Bloemen et al., 1988).

Acknowledgement. L.-Å.N. acknowledges financial support from the Swedish National Science Research Council. We thank J.G. Stacy for useful comments.

References

Bania, T.M.: 1986, *Astrophys. J.* **308**, 868
Bhat, C.L., Mayer, C.J., Wolfendale, A.W.: 1985a, *Nature* **314**, 511
Bhat, C.L., Mayer, C.J., Wolfendale, A.W. 1985b, *Proc XIX Int. Cosmic Ray Conf.* **1**, 336
Bhat, C.L., et al.: 1986, *Phil. Trans. R. Soc. London A* **319**, 249
Bignami, G.F., Fichtel, C.E.: 1974, *Astrophys. J. Letters* **189**, L65
Blitz, L., Bloemen, J.B.G.M., Hermsen, W., Bania, T.M.: 1985, *Astron. Astrophys.* **143**, 267
Blitz, L., Fich, M., Stark, A.A.: 1980, in *Interstellar Molecules* ed. B. Andrew, Reidel, Dordrecht, p. 213
Bloemen, J.B.G.M.: 1985, Thesis, University of Leiden
Bloemen, J.B.G.M., Blitz, L., Hermsen, W.: 1984a, *Astron. Astrophys.* **279**, 136 (Paper I)

Bloemen, J.B.G.M., Bennett, K., Bignami, G.F., Blitz, L., Caraveo, P.A., Gottwald, M., Hermsen, W., Lebrun, F., Mayer-Hasselwander, H.A., Strong, A.W.: 1984b, *Astron. Astrophys.* **135**, 12 (Paper II)

Bloemen, J.B.G.M., Caraveo, P.A., Hermsen, W., Lebrun, F., Maddalena, R.J., Strong, A.W., Thaddeus, P.: 1984c, *Astron. Astrophys.* **139**, 37

Bloemen, J.B.G.M., Reich, P., Reich, W., Schlickeiser, R.: 1988, *Astron. Astrophys.*, (in press)

Bloemen J.B.G.M., Strong, A.W., Blitz, L., Cohen, R.S., Dame, T.M., Grabelsky, D.A., Hermsen, W., Lebrun, F., Mayer-Hasselwander, H.A., Thaddeus, P.: 1986, *Astron. Astrophys.* **154**, 25 (Paper III)

Bloemen, J.B.G.M.: 1988, *Ann. Rev. Astron. Astrophys* (in press)

Bronfman, L., Cohen, R.S., Alvarez, H., May, J., Thaddeus, P.: 1988, *Astrophys. J.* **324**, 248

Dame, T.M.: 1983, Ph.D. Thesis, Columbia University

Dame, T.M., Thaddeus, P.: 1985, *Astrophys. J.* **297**, 751

Dame, T.M., Ungerechts, H., Cohen, R.S., de Geus, E., Grenier, I., May, J., Murphy, D.C., Nyman, L.-Å, Thaddeus, P.: 1987, *Astrophys. J.* **322**, 706

Gordon, M.A., Burton, W.B.: 1976, *Astrophys. J.* **208**, 346

Harding, A.K., Stecker, F.W.: 1985, *Astrophys. J.* **291**, 471

Heiles, C., Cleary, M.N.: 1979, *Australian J. Phys. Suppl.* **47**, 1

Heiles, C., Habing, H.J.: 1974, *Astron. Astrophys. Suppl.* **14**, 1

Henderson, A.P., Jackson, P.D., Kerr, F.J.: 1982, *Astrophys. J.* **263**, 182

Kerr, F.J., Bowers, P.F., Jackson, P.D., Kerr, M.: 1986, *Astron. Astrophys. Suppl.* **66**, 373

Kendall, M.G., Stuart, A.: 1973, *The Advanced Theory of Statistics*, Vol. II, Charles Griffin, London

Kulkarni S.R., Blitz, L., Heiles, C.: 1982, *Astrophys. J. Letters* **259**, L63

Kutner, M.L., Leung, C.M.: 1985, *Astrophys. J.* **291**, 188

Lebrun, F.: 1986, *Astrophys. J.* **306**, 18

Lebrun, F., Bennett, K., Bignami, G.F., Buccheri, R., Caraveo, P.A., Gottwald, M., Hermsen, W., Kanbach, G., Mayer-Hasselwander, H.A., Montmerle, T., Paul, J.A., Sacco, B., Strong, A.W., Wills, R.D. 1983, *Astrophys. J.* **274,** 231

Lester, D.F., Dinerstein, H.L., Werner, M.W., Watson, D.M., Genzel, R., Storey, J.W.V.: 1987, *Astrophys. J.* **320**, 573

Mayer-Hasselwander, H.A.: 1985, *Explanatory Supplement to the COS-B Database* (available from K. Bennett, Space Science Dept, ESTEC, Noordwijk, The Netherlands)

Reich, P., Reich, W.: 1988, *Astron. Astrophys.* (in press)

Solomon, P.M., Rivolo, A.R., Barrett, J., Yahil. A.: 1987, *Astrophys. J* **319**, 730

Stacy, J.G., Dame, T.M., Thaddeus, P.: 1987, *Proc. XX Int. Cosmic Ray Conf.* **1**, 117

Strong, A.W.: 1985a, *Astron. Astrophys.* **145**, 81

Strong, A.W.: 1985b, *Astron. Astrophys.* **150**, 273

Strong, A.W., Bloemen, J.B.G.M., Hermsen, W., Mayer-Hasselwander, H.A.: 1985, *Proc. XIX Int. Cosmic Ray Conf.* **1**, 317

Strong, A.W., Bignami, G.F., Bloemen, J.B.G.M., Buccheri, R., Caraveo, P.A., Hermsen, W., Kanbach, G., Lebrun, F., Mayer-Hasselwander, H.A., Paul, J.A., Wills, R.: 1982a, *Astron. Astrophys.* **115**, 404

Strong, A.W., Bloemen, J.B.G.M., Hermsen, W., Lebrun, F., Mayer-Hasselwander, H.A., Buccheri, R.: 1987, *Astron. Astrophys. Suppl.* **67**, 283

Strong, A.W., Riley, P.A., Osborne, J.L., Murray, J.D.: 1982b, *Monthly Notices Roy. Astron. Soc.* **201**, 495

Szabelski, J., Mayer, C.J., Richardson. K.M., Rogers, M.J., Wolfendale, A.W.: 1987, *Proc. XX Int. Cosmic Ray Conf.* **1**, 133

Swanenburg, B.N., Bennett, K., Bignami, G.F., Buccheri, R., Caraveo, P.A., Hermsen, W., Kanbach, G., Lichti, G.G., Masnou, J.L., Mayer-Hasselwander, H.A., Paul, J.A., Sacco, B., Scarsi, L., Wills, R.D.: 1981, *Astrophys. J. Letters* **243**, L69

Weaver, H.F., Williams, D.R.W.: 1973, *Astron. Astrophys. Suppl.* **8**, 1